Title
EXPERIMENTS ON SCATTERING OF 190 MEV DEUTERONS BY PROTONS

Author
Bloom, Arnold L.

Publication Date
1951-08-15

UCRL- 1442

UNIVERSITY OF CALIFORNIA — BERKELEY

RADIATION LABORATORY

DISCLAIMER

Unclassified-Physics Distribution
UCRL-1442

UNIVERSITY OF CALIFORNIA

Radiation Laboratory

Contract No. W-7405-eng-48

EXPERIMENTS ON SCATTERING OF 190 MEV DEUTERONS BY PROTONS

Arnold L. Bloom

(Thesis)

August 15, 1951

Berkeley, California

TABLE OF CONTENTS

EXPERIMENTS ON SCATTERING OF 190 MEV DEUTERONS BY PROTONS

I. Abstract

The total cross section for scattering of 190 Mev deuterons on protons and the differential cross section for certain types of inelastic deuteron-proton scattering, were measured in the external deuteron beam of the Berkeley synchrocyclotron. The total cross section was determined by measuring the differential cross section for scattering of charged particles from a hydrogen target; since any such collision, elastic or inelastic, will scatter two charged particles the integral of this cross section over all solid angles gives twice the total cross section desired. The cross section obtained in this way is $92 \pm 7 \times 10^{-27}$ cm^2, with Rutherford scattering excluded. Cross sections for inelastic scattering in which both protons suffer large changes of momentum have been examined by measuring coincidences between scattered protons; it is found that the protons are scattered nearly 90° apart in the laboratory system, with a narrow distribution in angle owing to the internal momentum of the deuteron. The differential cross sections for this process are summarized in Table II. Comparison of the experimental results is made with theory.

II. Introduction

Recent experiments in the high energy scattering of protons[1,2] and neutrons[3] show anomalies in the cross sections which to date have not been satisfactorily explained by theory. In particular, it is not yet clear whether the difference between the n-p and the p-p differential cross sections at energies of about 100 Mev and greater can be explained entirely in terms of the Pauli principle, assuming charge-independent forces, or whether there is also a charge-dependent effect. To the end of providing more information on this point, and particularly of determining indirectly the neutron-neutron interaction, a series of experiments has been instituted to determine the interaction of neutrons and protons with deuterons.[4,5,6]

The experiments to be described herein are part of this series and were designed to give the total cross section for scattering of 190 Mev deuterons on protons, and some information on the differential inelastic scattering cross sections of these particles. The experiments, performed in the external deuteron beam of the 184-inch Berkeley cyclotron, measured the total cross section by a direct charged particle count at various directions from a target in the beam. Information on certain phases of inelastic scattering was obtained by measuring coincidences between the two protons scattered in a collision when both protons, but not necessarily the neutron, suffered large changes in momentum. Such collisions will be called p-p type inelastic collisions; it is believed that conclusions drawn from p-p type collisions will also have some validity for n-p type collisions.

The principal conclusions are contained in Sections V and VII.

III. The Experimental Apparatus

A. Description of the Experimental Method

In these experiments we detected particles scattered from a target, placed in the deuteron beam of the cyclotron, with counters. To obtain the total cross section a count of all scattered charged particles was desired. It so happens, in a collision of a deuteron with a proton, that two and only two charged particles are scattered from the collision, whether or not the deuteron is broken up by the collision. (The neutron released in an inelastic collision goes practically undetected.) Thus, if the differential cross section is measured for charged particles scattered from a hydrogen target at various angles from the beam, the integral of the cross section over all solid angles will be exactly twice the total cross section for d-p scattering. This method of obtaining the total cross section may not be valid for nuclei other than deuterons and protons.

To determine the differential cross section $d\sigma/d\Omega$ for charged particles at an angle Φ we have a single counter defining a solid angle $\Delta\Omega$ at Φ. We are interested in knowing at what values of Φ we can find scattered particles. Theoretically, elastically scattered protons can be found for $0^\circ < \Phi < 90^\circ$, and deuterons for $0^\circ < \Phi < 30^\circ$. Inelastic particles are expected from 0° to about 80°, with a slight probability of being found to 90°. This theoretical distribution includes a small fraction of particles without enough energy to register in the detecting counter. It can be shown from energy and momentum conservation laws that, for deuterons incident on protons, two particles scattered from the same collision can never have an angle between them greater than 90°, and it follows as a corollary that no particle can be scattered at an angle greater than 90° from the beam.

The p-p type of collision was studied by looking for coincidences between the two protons. At deuteron energies of 190 Mev the de Broglie wavelength of the nucleons is small compared to the mean distance between particles in the deuteron, and we therefore expect that an inelastic collision will involve an interaction between only two particles; the third particle will continue in its trajectory little affected by the collision. For this reason the protons scattered in a p-p type collision will diverge at nearly right angles to each other in the laboratory system, where one proton is initially at rest. The scattering will not have exactly the same kinematics as expected in free p-p scattering, but will differ by a small amount owing to the internal momentum and binding energy of the deuteron. In particular, if one proton is scattered at an angle Φ to the beam, then the other proton will not be found at a unique angle, Θ, but may be found over a small range of angles Θ; furthermore, this proton may not be in the plane containing the beam and the other proton. The kinematics is discussed in detail in Section VI; here we summarize it in Fig. 1, which shows the beam and one counter at angle Φ, which is considered a point. The distribution in direction of the other proton is shown as a contour diagram on a sphere whose center is at the target., Points on a given contour line represent directions of equal probability (found experimentally as directions of equal coincidence counting rate). The contours are much wider vertically than horizontally and are symmetric about the plane containing the beam; the maximum counting rate is at the center.

The differential cross section, $d\sigma/d\Omega$, for p-p type scattering will be taken as the cross section, per unit solid angle, for scattering of one proton at an angle Φ irrespective of the exact direction of the other proton. This means that the scattering at angles Φ and Θ must be integrated over all angles Θ for which the scattering is p-p type. The directions of the charged particles in n-p type and elastic scattering are such that, in the majority of cases, there is no chance of mistaking collisions of these types with p-p type scattering.

We shall call the counter at angle Φ, which defines the solid angle, $\Delta\Omega$, used in calculating $d\sigma/d\Omega$, the "defining counter." The "non-defining counter" at angle Θ is moved about to give the coincidence counting rate as a function of position while the defining counter is held fixed.

The counters were stilbene crystals of various sizes, but usually of the order of 3 x 5 cm^2 in area and 1 cm thick. The hydrogen target was represented as the difference between a polyethylene target and a carbon target. The counters were usually from 50 to 100 centimeters from the target.

B. Electronics

A block diagram of the electronic arrangement is shown in Fig. 2. The two crystals are used in conjunction with 1P21 photomultipliers and distributed preamplifiers. The pulses are then amplified in distributed amplifiers and shaped by fast discriminators; the mixer circuit supplies coincidence and single counting rate pulses which are fed to conventional scalers. The single counting rate outputs are gated by a variable gate circuit, driven by a pulse circuit normally used to trigger the electric deflector of the cyclotron. Since the electric deflector is not used in these experiments the pulse circuit is available for this purpose and is so synchronized that the gate is opened about 100 µsec. before a burst of particles and remains open until about 100 µsec. after the burst. The fast pulse shapers are univibrators (Fig. 3); the coincidence circuit is distributed.[7,8]

The beam is monitored by an ionization chamber placed in the path of the beam and behind the rest of the apparatus. The chamber is filled with argon at a pressure slightly above atmospheric and has a collection distance between plates of two inches. The collecting field was 1000 volts per inch. The multiplication factor (ratio of positive charges produced in the chamber to incident particles) has been determined by Chamberlain, Segrè, and Wiegand[1] by calibrating against a Faraday cup beam collector built by Dr. V. Z. Peterson. The multiplication factor for 190 Mev deuterons is then obtained from the proton multiplication factor using the ratios of stopping powers of argon for the two particles.[9] The ionization chamber was used to charge a condenser whose voltage was measured by an electrometer circuit. The chamber and electrometer thus function as a beam integrator.

C. Other Details

1. The collimator

The collimator was a brass cylinder with internal diameter 1/2 inch for the first 35 inches and 3/4 inch for an additional 15 inches. A photograph of the beam taken just behind the collimator showed the beam surrounded by a weak "halo" of particles scattered near the end of the 1/2 inch section but not caught in the 3/4 inch section. The collimator was adjustable, and care was taken to be sure it was accurately parallel to the beam. The relative intensity of particles in the halo and in the beam has been determined by measuring film blackenings with a microphotometer; these measurements showed that not more than 0.1 percent of the particles are in the halo.

2. Aligning the scattering apparatus with the beam

The scattering apparatus was aligned to the beam by means of a moveable platform operated by remote control. Ionization chambers with split electrodes in which the upper and lower (or right and left) halves were of opposite polarity were used to monitor this operation. The electrometer circuits measured current differences between the two halves and correct alignment was indicated by zero current. The alignment was then checked by photographs of the beam at the front and rear of the scattering apparatus.

3. Scattering apparatus calibrations

The angles Φ and $(\Phi + \Theta)$ were marked in inscribed scales on the scattering apparatus itself. These scales have been checked by different observers at different times and are believed to be quite correct. Measurements of distances were usually made during an experiment by means of meter sticks.

4. Targets

The targets containing hydrogen were sheets of commercial polyethylene $(CH_2)_n$ and will be referred to hereafter as CH_2 targets. The carbon targets were graphite sheets machined to a thickness such that they had the same stopping powers as the CH_2 targets they were to match. Densities were determined after machining and cutting by measuring and weighing each target.

5. Cyclotron operation

The experiment utilized the external scattered deuteron beam of the 184-inch Berkeley cyclotron. The scattered beam was chosen in preference to the electrically deflected beam because it produces beam pulses from 50 to 100 microseconds long, as opposed to the electrically deflected pulses which are less than 10^{-7} seconds long. The longer beam pulse is essential in order that the true coincidences be observable above a background of accidental coincidences. The duty cycle (fraction of the time the cyclotron is actually putting out beam) varied from day to day, and, as the carbon subtraction depends on the duty cycle, it was necessary to calculate the carbon subtraction separately for each run. The cyclotron operating crew was under instruction to do nothing that would change the duty cycle during the day.

The energy of the beam has been investigated by obtaining a Bragg curve of the deuterons stopped by aluminum absorbers, according to a method described by Bakker and Segrè.[10] From these measurements the beam is believed to be nearly monoenergetic and to have a mean energy of 192 Mev.*

D. Tests

The following tests were made to insure that the scattering apparatus was measuring the desired effect:

1. The coincidence count per beam integrator unit for either elastic or inelastic scattering was measured as a function of the high voltage on one of the photomultipliers. The expected curve should have a platéau corresponding to conditions in which all heavy particles and a minimum of noise pulses are counted. A typical experimental curve is shown in Fig. 4. The voltage plateau is determined for each crystal independently.

2. In the case of d-p <u>elastic</u> scattering, coincidence counts from a hydrogen target can be expected only in the plane containing the beam and at certain definite angles Φ and Θ; at slightly different positions one can expect a reduced effect which should go to zero when no part of either crystal is in the correct position. The curves obtained by varying the height of the scattering apparatus and by varying the angle of one crystal are

* This point is discussed more fully in reference 6, which considers the same energy measurements employed for this experiment.

shown in Figs. 5 and 6 respectively. These curves convince us that the effect we are looking at is actually produced by a mechanism which operates according to the kinematics expected of d-p scattering. The variation of coincidence counting rate with position in the case of p-p type scattering is similarly in accord with kinematic predictions (Figs. 7 and 10).

E. Order of Events in Typical Run

1. The scattering apparatus and electronics were set up. The electronics were tested and the scaler discriminators set. The scattering apparatus was moved into rough alignment with the beam.

2. The cyclotron crew adjusted the cyclotron for optimum operation. Photographs of the beam as it leaves the collimator were taken and used in adjusting the collimator.

3. The scattering apparatus was aligned with the beam with the aid of the split ionization chambers and photographs.

4. The crystals were set at angles where previous experience had shown that a coincidence effect was easy to obtain. (For example, $\Phi = 45^\circ$, $\Phi + \Theta = 86^\circ$.) Photomultiplier voltage plateaus were then taken.

5. For inelastic scattering it was necessary to know the effective resolving time of the scalers and coincidence circuit. This was determined by using a carbon target and determining the counts per beam integrator unit as a function of beam intensity. This procedure is discussed more fully in Section IV.

6. The experimental data were then obtained. CH_2 and carbon targets were usually alternated in approximately five-minute intervals to minimize the effect of beam strength variations. The actual length of each

"run" was determined by the coincidence rate and the statistical accuracy desired.

IV. Analysis of Data

A. p-p Type Collisions

1. Corrections and uncertainties in the data

The counting rates of the individual counters are needed in the carbon subtraction calculation and may have to be corrected for the dead time of the scalers. If a scaler, counting a completely random source, has a dead time t, then the ratio of the observed counting rate to the true counting rate is given by

$$\frac{C_{obs.}}{C_{true}} \equiv \exp\left(-C_{true}\, t\right) \qquad (1)$$

To determine t for a scaler the logarithm of the counts per integrator unit, $\ln C_{obs.}/I$, is plotted as ordinate with the beam strength I (in terms of integrator units per second) as abscissa (Fig. 8). The points lie on a straight line which can be extrapolated to the limit of zero beam strength to give C_{true}/I. From (1) we have

$$t = \frac{\ln(C_{true}/I) - \ln(C_{obs}/I)}{I\,(C_{true}/I)} \qquad (2)$$

This value of t is essentially the true dead time divided by the effective duty cycle of the cyclotron. A chart giving the true counting rate as a function of both C_{obs} and t has been used to get C_{true}. It has been found that single counting rates of 150 per second require about 10 percent correction and experimental results are most consistent and reliable when the counting rate is kept below this value.

The actual dead time of the scalers for completely random pulses is about 0.5 microseconds. The dead time of the fast pulse shapers preceding the coincidence circuits is about 0.15 microseconds. At the counting rates employed no correction need be made for loss of coincidence counts caused by loss of counts in the fast pulse shapers.

The primary source of uncertainty in the original data is in the statistical character of the counting rates. Considerations of the amount of time available for use of the cyclotron permit us to get accuracies in the coincidence rates not better than 5 percent and usually between 5 percent and 10 percent. Uncertainties in beam integration, angle and distance measurements, target density and other fixed factors are of the order of 5 percent or less, and may be neglected for the time being.

2. The carbon subtraction

When the CH_2 target is used we may get coincidences from any one of three causes: (1) true coincidecnes from the hydrogen, which constitute the effect we are trying to measure, (2) true coincidences from scattering in the carbon, which, although usually small in number must be accounted for, and (3) accidental coincidences. When a carbon target is used we get coincidences from only (2) and (3); we therefore wish to obtain the hydrogen effect H, by subtracting the carbon coincidences from the CH_2 coincidences in some suitable fashion. To solve for H we have the following known quantities: m and n, the coincidence rates for C and CH_2 respectively, u_1, u_2, v_1, v_2, the single counting rates for the two crystals for C and CH_2 respectively, and τ, the effective resolving time of the coincidence circuit, such that the accidental coincidence rate is given by the usual formula $2u_1u_2\tau$. The data are taken in terms of counts per integrator unit for C and CH_2, say M and N respectively; we want a subtraction factor z such that

$$H = N - zM \quad . \tag{3}$$

The formula, derived in the appendix, is

$$z = A + \left(\frac{2\tau}{m}\right)\left(\frac{v_1v_2}{R} - Au_1u_2\right) \tag{4}$$

where A is the ratio of carbon density in CH_2 target to carbon density in C target (approximately 0.7) and R is the ratio

$$\frac{\text{integrator-units per seconds for } CH_2}{\text{integrator-units per second for C}} .$$

The resolving time τ is determined in the following way: the coincidence counts per integrator unit for carbon, M, $(=m/I_c)$ is plotted as a function of beam intensity, I_c (Fig. 9). The plot should be a straight line whose extrapolated value at zero beam intensity should give the true carbon coincidences M_o. The difference $(M - M_o)$ at a given value of I is produced by accidentals, so that $(M - M_o)I_c = 2u_1u_2\tau$ or

$$\tau = (M - M_o)I_c / 2u_1u_2 \qquad (5)$$

where u_1, u_2, M are at the value I_c.

The carbon subtraction taken in this way allows the value of z to be calculated individually for each pair of CH_2 - C data. If M, N, and τ have statistical uncertainties ΔM, ΔN, and $\Delta\tau$, then the uncertainty in H is given by

$$\sqrt{(\Delta M)^2 + (A\Delta N)^2 + (\Delta\tau)^2 \left(2I_c\left\{\frac{v_1v_2}{R} - Au_1u_2\right\}\right)} .$$

Since the correction term (the last term under the radical) is usually smaller than the others the uncertainty in H is approximately $\sqrt{(\Delta M)^2 + (A\Delta N)^2}$.

An alternative way of determining z, when single counting rates are not available, is to plot both M and N as a function of beam intensity. The ratio of the slopes of the M and N lines is then z, since N - zM must be independent of beam intensity. The uncertainties in H are usually in this case larger than with the previous type of carbon subtraction.

3. The cross section calculation

We wish to calculate the differential cross section in the laboratory system of coordinates, $d\sigma/d\Omega$, for all particles scattered in p-p type collisions for which one particle is scattered into the angle Φ. Let us first assume that we know the total counts per integrator unit, H^*, for particles scattered in this way. Then

$$\frac{d\sigma}{d\Omega} = \frac{7H^*}{DNT(\Delta\Omega)} \tag{6}$$

where D is the number of incident deuterons per integrator unit, N is Avogadro's number, T the effective density multiplied by the thickness of the CH_2 target, corrected if necessary in cases where the target is not perpendicular to the beam, and $(\Delta\Omega)$ is the solid angle subtended by the defining crystal. The factor 7 comes from the fact that 1/7 of the weight of the CH_2 target is hydrogen. If the integrator unit is 1 volt on the integrating condenser, then

$$D = C/M\epsilon \tag{7}$$

where C is the capacity, M the multiplication factor, of the chamber, and ϵ is the charge of the deuteron. M has been determined experimentally for a given density of argon in the chamber; it is corrected for the known density.

We now have to consider the method for obtaining H^*. As has been indicated earlier, the counterparts of the particles entering the defining crystal go into an elliptically shaped zone at approximately 90° to the defining angle, and the minor axis of the ellipse is in the plane of scattering. Early experiments having confirmed the narrowness of the ellipse, the entire ellipse was then covered in several vertical steps, each of which was wide enough to cover the whole horizontal width of the ellipse. Fig. 10 is a typical curve showing the effect, per integrator unit, as a function of the height of the non-defining crystal whose vertical width is h_o. Only the upper half of the ellipse can be covered, for mechanical reasons; a little bit of the lower half can be studied to check symmetry. The total area under the curve is therefore $2\int Hdh$ and the total counts under the ellipse $2\int Hdh/h_o$. The integration may be done by trapezoidal rule or similar method; the statistical accuracies involved do not require more refined methods.

If the ratio of H^* to the H at zero height, (H^*/H_p), is known at a given angle, Φ, say, it is given at other angles by the relation

$$(H^*/H_p)_{\Phi} = (H^*/H_p)_{\Phi_1} \quad \sin \Phi_1/\sin \Phi \tag{8}$$

This relation can be derived from Eq. (27). With its aid a cross section can be obtained for angles where a vertical distribution curve was not obtained experimentally.

Sample calculation.

(a) Calculation of a value of H from raw data. The following data was taken for $\Phi = 45^\circ$, $\Theta = 41^\circ$, $h = 0$,

crystals at angle Φ: area = 22.63 cm^2
distance from target = 95 cm

crystals at angle Θ: area = 36 cm^2
height h_o = 1.73 inches
distance from target = 50 cm
horizontal angular width about 10°

Targets: CH_2: thickness ; 0.283 grams/cm^2 } perpendicular to beam
C: thickness = 0.336 grams/cm^2 }

Integrating condenser: 0.102 microfarads

Multiplication factor of chamber: 1806

$\tau = 1.5 \times 10^{-5}$ seconds.

Raw data:

Target	Time seconds	Total Counts Φ	Total Counts Θ	Total Counts coinc.	Integrator units volts
CH_2	264	3231	18702	100	2.0
C	142	1439	8144	9	1.0
none	63	302	1343	2	0.5

At these counting rates no single count corrections are necessary.

Carbon subtraction calculation.

$A = 0.722,\ 2\tau = 3.0 \times 10^{-5},\ R = 1.08,\ m = 9/142 = 0.0634$

$u_1 = 10.1,\ v_1 = 12.2,\ u_2 = 57.3,\ v_2 = 70.8$

$$z = A + \frac{2\tau}{m}\left(\frac{v_1 v_2}{R} - Au_1u_2\right) = 0.722 + 0.167 = 0.889$$

Thus we take $H = (50 \pm 5) - (8 \pm 2) = (42 \pm 5)$.

(b) Calculation of $d\sigma/d\Omega$. Let us take the curve drawn in Fig 10, as the curve to be integrated. For $h_o = 1.73$ inches $H^* = 132$. Then

$D = C/M\varepsilon = (1.02 \times 10^{-7})/(1806 \times 1.6 \times 10^{-19})$

$D = 3.53 \times 10^8$ deuterons per integrator volt.

$d\sigma/d\Omega = 7H^*/DN\,T(\Delta\Omega)$, where

$H^* = 132,\ D = 3.53 \times 10^8,\ N = 6.02 \times 10^{23},\ T = 0.283$

$(\Delta\Omega) = 22.36/(95)^2 = 0.0025$ giving $d\sigma/d\Omega = 6.1 \times 10^{-27}\ cm^2$, with an accuracy of about 10 percent.

B. Total Scattering

1. Corrections of uncertainties in the data

The considerations for loss of counts in the scalers discussed in Section IV-A also apply here. The discussion of uncertainties in the data applies, except that better statistical accuracy can usually be expected owing to the greater counting rates obtained in the single counters.

2. Carbon subtraction

As we are here concerned with single counts, rather than coincidences, we wish to subtract off the counts due to carbon directly. The effect, (H), is therefore equal to N - AM - (1 - A)(Bl), where the symbols have the same meaning as in paragraph A2 of this section. (Bl) is the count per integrator unit when there is no target in place. The extra correction comes about from the fact that the same no-target effect is being counted for both the CH_2 and C targets.

3. The cross section calculation

The effect, H, for single counts at a given angle, Φ, gives the differential cross section at that angle by the same formula used in paragraph A3, namely

$$d\sigma/d\Omega = \frac{7H}{DNT(\Delta\Omega)} \tag{6}$$

The integral of $d\sigma/d\Omega$ taken over the sphere, $2\pi\int_0^\pi d\sigma/d\Omega \sin\Phi\, d\Phi$, is the cross section for charged particles scattered into the sphere. Since any collision, elastic or inelastic, will scatter two charged particles, this cross section is just twice the actual total cross section for d-p scattering. We have, therefore

$$\sigma = \pi \int_0^\pi d\sigma/d\Omega \sin\Phi\, d\Phi \quad . \tag{8}$$

In the laboratory system of coordinates $d\sigma/d\Omega$ is theoretically zero for $\Phi > \pi/2$. The integration is done by one of the usual numerical methods.

The details of the integration will be discussed in Section V-B. For comparison with total cross section obtained in this way we have the total cross section for 90 Mev neutrons on deuterons, obtained experimentally from beam attenuation measurements.[11,12] We expect our result to be similar.

V. Results

A. Inelastic Cross Sections

The inelastic cross sections at various values of Φ are listed in chronological order in Table I; the weighted mean averages are shown in Table II and Fig. 11. The mean errors listed in Table I are estimates based on the possible variations in H^* one can obtain while remaining within the statistical accuracies of the individual values of H. The statistical uncertainties in H, examples of which can be seen in Fig. 10, are compounded of the statistical uncertainties of the CH_2 and C counting rates, with a small additional uncertainty in the carbon subtraction factor. Systematic errors in beam integration, target thicknesses, etc., are not included but are believed to be small compared to other sources of error.

At $\Phi = 30°$ it will be noticed that the cross section obtained with a CH_2 target 0.283 g/cm^2 thick is distinctly smaller than that obtained with a thinner target. The mean energy of the inelastic particles scattered to $\Theta = 55°$ is about 25 Mev, with a range of about 0.7 g/cm^2 of carbon.[9] Since the particles must pass through approximately the equivalent of 0.45 g/cm^2 of carbon before reaching the crystal it is evident that there will be a fair number of particles with insufficient range to produce a countable pulse in the crystal. For this reason we have decided not to include the thick target data in Table II. At $\Phi = 25°$ the mean energy of the Θ particles is about 20 Mev, with a range of about 0.45 g/cm^2 of carbon, and we therefore assume that we did not count all the low energy particles, even though thin targets were used. We believe the true cross section at 25° may be between 7.5 and 8 millibarns per unit solid angle.

The largest sources of systematic error, apart from loss of low energy particles, is uncertainty as to the exact zero height position of the

Table I. Chronological List of Inelastic Cross Sections

Date	Φ^{o}	$d\sigma/d\Omega$, millibarns	Density of CH_2 Target grams/cm^2
3-9-51	45	5.3 ± 0.8	0.283
4-16-51	45	6.3 ± 0.7	0.283
5-17-51	45	5.3 ± 0.5	0.283
5-17-51	30	5.4 ± 0.5	0.283
6-13-51	30	7.4 ± 0.7	0.072
6-31-51	45	6.1 ± 0.6	0.283
6-31-51	37	6.0 ± 0.9*	0.283
6-31-51	30	5.7 ± 0.8*	0.283
6-31-51	30	7.0 ± 1.0*	0.072
6-31-51	25	6.3 ± 1.2*	0.072

* assumes the theoretically predicted vertical distribution

Table II. Weighted Average Values of the Inelastic Cross Sections

Φ^{o}	$d\sigma/d\Omega$, millibarns per unit solid angle
45°	5.7 ± 0.2
37°	6.0 ± 0.9
30°	7.3 ± 0.6 Thin targets only
25°	6.3 ± 1.2

crystal. The effect of this uncertainty will be greatest at $\Phi = 45^\circ$, where it may be as much as 10 percent.

B. The Total Scattering Cross Section

The total cross section for d-p scattering is, strictly speaking, infinite because part of it is due to Rutherford scattering. However, the Coulomb forces affect the cross section markedly only at very small angles of deflection in the center-of-mass system, and this effect is only in the elastic scattering. Therefore, if we agree to include in the total cross section only those particles scattered by essentially nuclear effects, we not only get a finite cross section but one that can be compared directly with neutron-deuteron cross sections. We therefore define our cross section to include all inelastic scattering and all elastic scattering in which the angle of deflection in the center-of-mass system is greater than 10 degrees. To obtain this cross section we calculated $\frac{1}{2}\int_0^{\pi/2} 2\pi \frac{d\sigma}{d\Omega} \sin\Phi \, d\Phi$ using the following function for $d\sigma/d\Omega$:

1. From $\Phi > 3.3^\circ$ (10° in the center-of-mass system), to $\Phi = 70^\circ$ $d\sigma/d\Omega$ is the value obtained from the total cross section experiments described previously. (Table III)

2. From $\Phi = 70^\circ$ to $\Phi = 85^\circ$, $d\sigma/d\Omega$ is the cross section for elastic scattering of protons. (Table III) The experimental points were obtained by observing the corresponding high energy deuterons at small angles, with lower energy particles screened out by absorbers.[6]

3. From $\Phi = 85^\circ$ to 90° the only particles expected in significant numbers are protons scattered elastically at less than 10° in the center-of-mass system. In view of the cutoff mentioned above, we take $d\sigma/d\Omega$ to be zero in this region.

Table III. Values of $2\pi \sin \Phi \frac{d\sigma}{d\Omega}$, mb., for Charged Particles

0°	Date 4-16-51	Date 5-28-51	Elastic Scattering	Value used in integration
5		262 ± 60		285
8	300 ± 50	374 ± 35		300
10		296 ± 13		296
15	228 ± 20	224 ± 16		230
20		142		180
25	125	142		132
30		91		106
35	98			90
40		69		84
45	87	80		80
50		76		74
55	67			70
60		66		62
65	48	55		51
70		33	45	46
75	3	3	50 ± 4	52
80		3		67
82	1		71 ± 6	
85				70

4. At $\Phi = 3.3^\circ$, the cutoff angle for high energy deuterons in the laboratory system, we must subtract the contribution from the elastic cross section. The value of the elastic cross section at this point is taken from Stern.[6] There is thus a discontinuity in the curve between values of $d\sigma/d\Omega$ at Φ less than and greater than 3.3°.

5. For $0^\circ < \Phi < 3.3^\circ$, $d\sigma/d\Omega$ is not expected to vary greatly and $\sin\Phi$ is the governing term in the integration. We therefore take $2\pi \sin\Phi \frac{d\sigma}{d\Omega}$ to rise linearly from zero at 0° to its value at Φ just less than 3.3°.

The experimental points and curve of integration are shown in Fig. 12 and Table III. The value of σ obtained in this way is $\sigma = (92 \pm 7) \times 10^{-27}$ cm^2, the uncertainty being compounded of statistical errors and uncertainties in the experimental arrangement.

There are two primary sources of error as a result of particles not being counted in the experiment. They are, (1) protons between 0° and 5° produced by "stripping" (n-p type collisions), and (2) low energy inelastic particles in the region 50° to 90°. The effect of (1) can be estimated from the observed stripped particle distribution[13] and the theoretical estimated cross section for small-angle protons (Table VII). We estimate that this effect may increase the cross section by not more than one millibarn. The effect of (2) can be estimated by smoothing the dip in the experimental curve at $\Phi = 70^\circ$; it is also about one millibarn.

We conclude that the total cross section for d-p scattering at 190 Mev is $(92 \pm 7) \times 10^{-27}$ cm^2. The corresponding value for n-d scattering is given in references 11 and 12 as $(117 \pm 5) \times 10^{-27}$ cm^2 and $(105 \pm 4) \times 10^{-27}$ respectively.*

---

* In reference 11 the author believes the figure of 117 millibarns was for neutrons whose average energy was 83 Mev. The figure of 105 millibarns was for 95 Mev neutrons.

VI. Theory

A. Kinematics of Inelastic Scattering

In this section we wish to predict where the particles scattered in a collision will go; in other words, we expect to get all the information about the scattering except the actual magnitude of its cross section. We will assume, to simplify calculation, that the mechanics of the collision can be completely accounted for by the collision of the target particle with one particle in the deuteron, with the absorption of the deuteron binding energy between these two particles; the third particle is supposed to leave the collision with the same momentum it had just prior to the collision.

1. Simplified case

Let us assume a collision in which the particles in the deuteron have zero internal momentum. Let the deuteron have a kinetic energy 2E, so that the colliding particle has a momentum, p, corresponding to a free particle with energy E. Let B be the binding energy of the deuteron. Consider the center-of-mass system of the two colliding particles only. In this system each particle before collision has momentum p corresponding to free particles of energy $E/4$. After collision the particles actually are free and each particle has energy $(E/4 - B/2)$ with corresponding momentum which we will call p'. Let X be the angle of deflection in the c.m. system (Fig. 13) and Φ and Θ the angles in the laboratory system. Then, non-relativistically,

$$\operatorname{ctn} \Phi = \operatorname{ctn} X + (p/p') \csc X \tag{10}$$

$$\operatorname{ctn} \Theta = -\operatorname{ctn} X + (p/p') \csc X \tag{11}$$

We can eliminate X by solving explicitly for ctnX and cscX and using $\csc^2 X - \operatorname{ctn}^2 X = 1$. The result is

$$\frac{1}{2}\left[1 + (p'/p)^2\right] \operatorname{ctn}\Phi \operatorname{ctn}\Theta - \frac{1}{4}\left[1 - (p'/p)^2\right] (\operatorname{ctn}^2\Phi + \operatorname{ctn}^2\Theta) = 1 \tag{12}$$

To simplify this relationship let us take the factor which perturbs the scattering from free-particle scattering as a small quantity. We define

$$\varepsilon = \frac{1}{2}\left\{1 - (p'/p)^2\right\} = B/E \tag{13}$$

and expand (12) as a power series in ε. The result is

$$\text{ctn}\,\Theta = \tan\Phi\left\{1 + \varepsilon + \frac{\varepsilon}{2}(\text{ctn}^2\Phi + \text{ctn}^2\Theta) + O(\varepsilon^2)\right\} \tag{14}$$

We neglect terms of order ε^2 and higher because ε is about 0.02. For calculation it is convenient to use a trial value of $\text{ctn}^2\Theta$ on the right hand side of (14), say $\text{ctn}^2\Theta = \tan^2\Phi$ (free particle scattering). Successive improvements can be made by substituting the value of ctn Θ thus obtained into the right hand side of the next approximation.

The relativistic correction is made by using relativistic addition of velocities to derive equations similar to (10) and (11). The effect on (14) is that ctn Φ and ctn Θ must be replaced by $(1 + \beta)$ ctn Φ and $(1 - \beta)$ ctn Θ, respectively, wherever they occur. $c\beta$ is the velocity before collision. In this experiment β is about 0.3 and the correction is small.

Table IV shows the values of Θ and $\Phi + \Theta$ obtained in this way for representative values of Φ. Note the very slow variation of $\Theta + \Phi$ with Φ. E = 95 Mev, B = 2.2 Mev.

Table IV. Θ as a Function of Φ

$\Phi°$	$\Theta°$	$(\Phi + \Theta)°$
11.3	71.6	82.9
20	65.8	85.8
30	57.0	87.0
37	50.2	87.2
45	42.5	87.5

2. Maximum angle and energy of particles

According to Fig. 13 there must be a maximum angle in the laboratory system, Φ_{max}, beyond which particles cannot be scattered. At this angle $\Phi + (\pi - X) = 90^{\circ}$, so, obviously,

$$\cos \Phi_{max} = \sqrt{\frac{p^2 - p'^2}{p^2}} = \sqrt{\frac{2B}{E}} = \sqrt{2\mathcal{E}} \tag{15}$$

For the constants used above Φ_{max} is about 73°.

The energy of the (high energy component) particles at small angles of Φ is approximately

$$E_{\Phi} \approx E \cos^2 \Phi - B/2 \tag{16}$$

At Φ_{max} the energy is

$$E_{\Phi max} = 1/2m(p^2 + p'^2) = B/2 \tag{17}$$

3. Effect of internal momentum

Let us define the coordinate system, x, y, z, as follows: z is the direction of the incident beam, x is perpendicular to the beam, and in the plane defined by the beam and the defining crystal, y is perpendicular to this plane. We will consider the effect of the internal momentum components p_z, p_x, p_y in that order.

(a) Effect of p_z. The effect of this component, since it is in the direction of the incident motion, is to change the apparent energy of the colliding particles. We will consider E a variable, $E = (2p + p_x)^2/2m$ instead of $2p^2/2m$ as before, as p_x is a variable. We are interested in $d\Theta/dE$ for a fixed Φ.

$$\frac{d\Theta}{dE} = \frac{d\Theta}{d\mathcal{E}} \cdot \frac{d\mathcal{E}}{dE} , \quad \frac{d\mathcal{E}}{dE} = -\frac{B}{E^2}$$

By differentiating (14) we get

$$-\csc^2 \Theta \ \frac{d\Theta}{dE} = \tan \Phi \left[\frac{1}{2} + \frac{1}{4} (\mathrm{ctn}^2 \Phi + \mathrm{ctn}^2 \Theta) + O(\varepsilon) \right] \tag{18}$$

so that, for Θ in degrees,

$$d\Theta/dE = (180/\pi)(B/E^2) \tan \Phi \sin^2 \Theta \left[\frac{1}{2} + \frac{1}{4} (\mathrm{ctn}^2 \Phi + \mathrm{ctn}^2 \Theta) \right] \tag{19}$$

For energies in the region of 100 Mev the variation of Θ with energy is small. To see within what limits we can expect Θ to vary, let us consider the momentum distribution inside the deuteron. According to Serber[13] the probability per unit kinetic energy range P (E) dE is, in our notation,

$$P(E)dE = \left\{ \sqrt{2BE_p}/\pi \left[(E - E_p)^2 + 2BE_p \right] \right\} dE \tag{20}$$

where E_p is 1/2 the energy of the deuteron, 95 Mev. As a temporary criterion let us take $E(^{max}_{min})$ as $(\sqrt{E_p} \pm \sqrt{B})^2$; the probability at these points is about 1/10 the peak probability. With these values we design Table V.

Table V. Effect of Internal Momentum

$\Phi°$	$(\Phi + \Theta)°$		
	E_{min}	E_p	E_{max}
45	87.3	87.5	87.6
30	86.6	87.0	87.2
20	85.3	85.8	86.0

We conclude that the p_z component of internal momentum spreads Θ into a very small region. In the event there are significant probabilities for large internal momenta (about $\sqrt{2mE_p}$) the $1/E^2$ dependence of $d\Theta/dE$ provides that there will be a sharp cutoff for increasing Θ but a long tail at smaller values of Θ.

(b) Effect of p_x. The effect of internal momentum perpendicular to the beam direction is effectively to change the direction of the incoming particle at the moment of collision. This direction makes an angle α with the beam such that $\tan \alpha = p_x/\sqrt{2mE_p}$, and the angle Φ of the defining crystal is really, from the point of view of this collision, $\Phi + \alpha$. To see what effect this has on Θ, we again consider Serber's momentum distribution of the deuteron, in terms of probability per unit momentum range.

$$P(p_x)dp_x = \left[\sqrt{mB} / \pi (mB + p_x^2)\right] dp_x \qquad (21)$$

As a temporary indication of the spread in α, let us take p_x at $\pm \sqrt{2mB}$. At these points the curve is 1/5 the peak value and the probability of finding p_x within these limits is about 0.6. The corresponding value of $\tan^{-1} \sqrt{B/E}$, is $8.7°$. We now look again at Table IV, keeping in mind that for a defining crystal at angle Φ we must look for values of $(\Phi + \Theta)$ corresponding to $\Phi \pm \alpha$ instead of Φ alone. It is obvious that for $\Phi = 30°$ and $45°$ the spread in $\Theta + \Phi$ is very small, of the order of one degree for the entire momentum distribution. For $\Phi = 20°$ the spread is larger, about $5°$ for the main body of the curve with a sizeable tail extending to smaller values of $\Phi + \Theta$. Unfortunately this tail will be difficult to determine experimentally because elastic scattering also occurs near this combination of Φ and Θ.

(c) The effect of p_y is again to change the direction of the incoming particle, this time to tilt the plane of scattering. The situation is illustrated in Fig. 14. Here the target is O, the defining crystal at A, the beam direction is Oz, and the "original plane" of the scattering table (as used for elastic scattering, for example) is OAz. We now assume an incident particle in the direction Oz', making an angle

K ($= \tan^{-1} p_z/\sqrt{2mE_p}$) with Oz. The partner of the particle scattered to A goes to B', whose projection on the plane OAz is B. We define our angles as follows:

$$K = \angle zOz' \qquad \mu = \angle BOB' \qquad \Phi = \angle zOA$$

$$\Phi' = \angle z'OA \qquad \Theta = \angle zOB \qquad \Theta' = \angle z'OB'$$

Let ν be the angle of inclination between planes OAz and OAz'. Since the line of intersection of these planes is OA we can write

$$\tan K = \tan \nu \sin \Phi \tag{22}$$

$$\tan \mu = \tan \nu \sin (\Phi + \Theta) \tag{23}$$

therefore $\tan \mu/\tan K = \sin (\Phi + \Theta)/\sin \Phi$ (24)

or, approximately,

$$\tan \mu = \tan K/\sin \Phi \tag{25}$$

The relations between Φ', Θ' and Φ, Θ are given by

$$\cos \Phi' = \cos \Phi \cos K \tag{26}$$

$$\cos (\Phi' + \Theta') = \cos (\Phi + \Theta) \cos \mu \tag{27}$$

In the experiment Φ is fixed, $(\Phi' + \Theta')$ must satisfy (14), μ may be varied by changing the height of the nondefining crystal, and $(\Phi + \Theta)$ is the angle between the arms of the scattering table. Table VI gives the relations between these angles for $p_y = \sqrt{2mB}$, ($K = 8.7°$). <u>h</u> is the height above normal in inches, of the nondefining crystal when the crystal is 50 cm from the target. These peculiar units are used because it is convenient to measure the lengths this way during an experiment.

Table VI. Vertical Effect

$\Phi°$	$\Phi'°$	$(\Phi' + \Theta')°$	$(\Phi + \Theta)°$	$\mu°$	h"
45	45.8	87.5	87.3	12.3	4.3
37	38.0	87.2	87.0	14.3	5.0
30	31.2	87.0	86.8	17.1	6.0
20	21.8	86.0	85.7	24.2	8.9

In summary, we can see from Tables V and VI that the distributions will be wide vertically and narrow horizontally. The sharp cutoff on the wide angle side of the distribution will, in the experiment, be spread out owing to the finite size of the crystals. It should be pointed out that the unsymmetrical character of the horizontal distribution shifts the centroid of the curve to the small angle side of the peak, so a large crystal set at the "center" of the curve will actually have to be set several degrees less than the peak values given in Table IV.

B. Comparison of Experimental Results with Theory

The theory of high energy nucleon-deuteron scattering has been studied, by means of the Born and impulse approximations, by Chew,[14,15,16] Gluckstern and Bethe,[17] and others. At this date quantitative predictions are available for the differential cross section for elastic scattering,[6,14] for the total cross sections of various types of inelastic scattering, and for the over-all total cross section.[17] We shall attempt to compare our results with whatever is available in the way of quantitative theoretical predictions.*

In Fig. 15 the differential cross sections for four types of scattering are shown in the <u>laboratory</u> system of coordinates. The curves represent, (1) the cross sections for free n-p scattering with incident 90 Mev neutrons.[3] The total cross section for this process is about 73 millibarns.[12] (2) The cross section for free p-p scattering at about 90 Mev, based on a uniform differential cross section of 5.5 millibarns per unit solid angle in the center-of-mass system.[2] The total cross

---

* As a working hypothesis we shall assume that n-n forces are the same as p-p forces, so that predictions for n-d scattering can be carried over to d-p scattering unchanged except for the substitution of the word "proton" for "neutron," and vice versa.

section obtained on the basis of this assumption (excluding Rutherford scattering, of course) is 38 millibarns. (3) The cross section for the inelastic p-p type collisions, with points from 25° to 45° extrapolated to the complementary points beyond 45°. (4) A curve obtained by subtracting, from the differential cross section for charged particles, the differential cross section for p-p type scattering and elastic scattering.[6] This curve should in principle give the differential cross section for n-p type inelastic scattering, since other types of scattering have been accounted for.

An examination of these curves shows that, in the region of angles corresponding to the largest momentum transfers, the inelastic p-p and n-p curves have approximately the same shape as the corresponding free-particle curves, but whereas the p-p scattering is suppressed to one-third its free-particle values the n-p curve apparently shows no such suppression. This result is suprising for two reasons; first, because there is no reason in theory to expect only the p-p type of scattering to be suppressed, and secondly because, as Gluckstern and Bethe[17] pointed out, the n-p type of scattering is expected to be suppressed because there is interference between the exchange scattering of the direct and antisymmetrized protons by the neutron. We are inclined to believe that the discrepancy between theory and experiment here is the result of an incomplete integration of the p-p type particles rather than a defect in the theory. An incomplete integration could be explained by the possibility that many particles have insufficient energy to register in the counters, or that some particles, coming from collisions in which the deuteron had a high internal momentum, fell outside the main groups examined by the crystals.

The other points at which the inelastic curves depart from the free-particle curves are fairly easily explained. The inelastic n-p curve, at large angles, and the inelastic p-p curve, at small and large angles, are both expected to be low because they correspond to collisions in which the neutron and one proton go off with nearly the same momentum, and such collisions are most easily "robbed" by elastic scattering. At angles of 20^{o} and less the curve obtained by subtracting p-p type and elastic scattering no longer represents n-p type scattering because it includes many stripped protons.

In Table VII are shown the principal conclusions reached by Gluckstern and Bethe,[17] listed in their system (90 Mev neutrons incident on deuterons) and in our system (190 Mev deuterons incident on protons). The values for δ of 1, 0, and -1 correspond to ordinary, Serber and exchange forces respectively; previous experiments[3,4] indicate that the Serber force most nearly agrees with experimental results. We shall consider here the comparison between the total cross section for p-p type collisions (in our system) and free p-p collisions. According to the theory the cross sections should be about 19 and 30 millibarns respectively.* From experiment they are estimated to be about 15 and 38 millibarns respectively. Since the 15 millibarn figure is a lower limit the agreement between theory and experiment may be considered fair.

---

* This number was obtained on the basis of total n-d and n-p cross sections of 117 and 83 millibarns respectively.[11] In the light of more recent experiments[12] the numerical conclusions of Gluckstern and Bethe probably need revision.

Table VII. Calculated Total Cross Sections* - Gluckstern and Bethe

G and B's System	$\delta=1$	0	-1	Our System
N-N force	1	1/2(1+P)	P	p-p force
Total elastic	80	60	30	Total elastic
Elastic giving low energy deuterons	65	50	30	Elastic at small angles
Low energy protons	1	19	50	Small angle neutrons ($\sim 10^{\circ}$) or p-p type collisions
N-N cross section	20	30	62	Free p-p cross section
High energy protons	approximately 20			Small angle protons ($\sim 10^{\circ}$)

* in millibarns

VII. Conclusions

1. The differential cross section for inelastic p-p type scattering has been measured at certain angles of deflection and found to be about one-third the corresponding cross section for free p-p scattering. This value is lower than that expected from theory; however, since the cross section determined in this experiment is a lower limit, the disagreement between theory and experiment may not be as bad as it appears at first sight. The angular distribution of these inelastically scattered particles is adequately predicted by a kinematical theory which assumes that one of the three nucleons involved in the collision escapes with no change in energy and momentum.

2. The total scattering cross section for d-p scattering has been measured and found to be 92 ± 7 millibarns, when a suitable cutoff is used for elastic scattering to eliminate divergences produced by Coulomb forces. This figure is again a lower limit, but the upper limit, aside from statistical considerations and dependence on the cutoff angle, is probably not more than 2 millibarns above the lower limit. This cross section is comparable to the corresponding neutron-deuteron total cross section.

3. By subtracting the elastic and p-p type scattering from the total scattering we have obtained an upper limit for the inelastic n-p type scattering over a limited range of angles. The upper limit differential cross section thus obtained is approximately the same as for free n-p scattering.

4. We believe that the results of these experiments are not inconsistent with the assumption of charge-independence of nuclear forces; however, much more experimental work has to be done before any definite conclusions on the nature of nuclear forces can be reached.

VIII. Acknowledgements

Thanks are due Professors Owen Chamberlain and Emilio Segrè for suggesting this experiment, and for their continued aid and encouragement during its development. Appreciation should be expressed to Dr. C. Wiegand, who kindly loaned certain electronic equipment and gave advice, to Dr. R. F. Leininger, who kindly crystallized and cut the stilbene crystals, to the crew of the 184-inch cyclotron for their patience and expert advice in the operation of the cyclotron, and to those graduate students who from time to time assisted in the experimental operations. Finally we wish to express great appreciation to Mr. Martin O. Stern, whose assistance and advice on all phases of the experiment helped shorten the hours of cyclotron operation, calculation and equipment maintenance, and made the experiment possible.

This work was performed under the auspices of the Atomic Energy Commission.

IX. Bibliography

1. O. Chamberlain and C. Wiegand, Phys. Rev. 79, 81 (1950); O. Chamberlain, E. Segrè, and C. Wiegand (to be published).

2. R. Birge, U. Kruse, and N. Ramsey, Phys. Rev. 83, 274 (1951).

3. E. Kelly, C. Leith, E. Segrè and C. Wiegand, Phys. Rev. 79, 96 (1950); J. Hadley, E. Kelly, C. Leith, E. Segrè, C. Wiegand and H. York, Phys. Rev. 75, 351 (1949).

4. Wilson M. Powell (to be published).

5. M. Stern and A. Bloom, Phys. Rev. 83, 178 (1951).

6. M. Stern, thesis, University of California (Sept. 1951), UCRL-1440, (to be published).

7. E. Ginzton, W. Hewlett, J. Jasberg, and J. Noe, Proc. I.R.E. 36, 956 (1948).

8. C. Wiegand, Rev. Sci. Inst. 21, 975 (1950).

9. W. Aron, B. Hoffman, and F. Williams, Range-Energy Curves, AECU-663 (UCRL-121 2nd Rev.), unpublished.

10. C. Bakker and E. Segrè, Phys. Rev. 81, 489 (1951).

11. L. Cook, E. McMillan, J. Peterson and D. Sewell, Phys. Rev. 75, 7 (1949).

12. J. DeJuren and N. Knable, Phys. Rev. 77, 606 (1950).

13. R. Serber, Phys. Rev. 72, 1008 (1947).

14. G. F. Chew, Phys. Rev. 74, 809 (1948).

15. G. F. Chew, Phys. Rev. 80, 196 (1950).

16. G. F. Chew (to be published).

17. R. Gluckstern and H. Bethe, Phys. Rev. 81, 761 (1951).

APPENDIX

Derivation of the Carbon Subtraction Equation for Section IV-A

1. Definition of symbols used.

A = (mass of carbon in CH_2 target) / (mass of carbon in C target)

a_1, a_2 = single counting rates (counts per second) for the single counters for C target, excluding all single counts which are the result of <u>true</u> coincidences.

b_1, b_2 = single counting rates from hydrogen in the CH_2 target, excluding those which are the result of true coincidences.

I_c = beam strength for C target in terms of integrator units per second.

I_H = beam strength for CH_2 target.

m = coincidence rate (counts per second) with C target.

n = coincidence rate with CH_2 target.

R = I_H/I_c .

u_1, u_2 = actual single counting rates for the two counters for C after correction for counting losses in the scalers themselves.

v_1, v_2 = actual single counting rate for CH_2 target.

x = true coincidence rate for C target.

y = true coincidence rate from hydrogen in the CH_2 target.

z = carbon subtraction ratio.

z' = carbon subtraction ratio from simplified derivation.

τ = effective resolving time of coincidence circuit in seconds.

2. Simplified derivation, assuming constant beam intensity.

$(I_H = I_c)$

The experimental data are $u_1, u_2, v_1, v_2, m, n,$ and τ. The unknowns are a_1, a_2, b_1, b_2, x and y. The relations between unknown and data are

$$\text{(i)}\quad u_i = a_i + x \qquad \text{(ii)}\quad v_i = A(a_i + x) + b_i + y$$

$$\text{(iii)}\quad m = x + 2\tau a_1 a_2 - O(\tau^2)$$

$$\text{(iv)}\quad n = y + Ax + 2\tau(b_1 b_2 + A^2 a_1 a_2 + A\, a_1 b_2 + A a_2 b_1 - Axy) - O(\tau^2)$$

Now it is found experimentally that

$$\text{(v)}\quad x, y \ll a_1, a_2, b_1, b_2$$

$$\text{(vi)}\quad 2\,Axy \ll \text{other terms of order } \tau .$$

Also, since τa_i and $\tau b_i \ll 1$, all terms of order τ^2 are very small. Thus by neglecting small terms we can simplify the relations to the following:

$$\text{(vii)}\quad u_i = a_i \qquad \text{(viii)}\quad v_i = Aa_i + b_i \qquad \text{(ix)}\quad m = x + 2\tau a_1 a_2$$

$$\text{(x)}\quad n = y + Ax + 2\tau(b_1 b_2 + A^2 a_1 a_2 + Aa_1 b_2 + Aa_2 b_1) .$$

We can immediately rewrite (ix) as (xi) $x = m - 2\tau u_1 u_2$

and, substituting (vii), (viii) and (xi) into (x) we obtain

$$\text{(xii)}\quad y = n - Am - 2\tau(v_1 v_2 - A\, u_1 u_2)$$

If we write $y = n - z'm$, it follows that

$$\text{(xiii)}\quad z' = A + (2\tau/m)(v_1 v_2 - Au_1 u_2) .$$

3. Derivation for the case where I_c and I_H differ by a small factor (as usually happens during an experiment).

If the beam strength varies the counting rates will also vary; however we expect the <u>counts per integrator unit</u> a_i/I_c, b_i/I_H, x/I_c and y/I_H to be constant because they depend only on a cross section in the target materials. Let us first divide (xi) by I_c and (xii) by I_H. We get

$$\text{(xiv)} \quad x/I_c = m/I_c - 2\tau u_1 u_2/I_c$$

$$\text{(xv)} \quad y/I_H = n/I_H - Am'/I_H - (2\tau/I_H)(v_1 v_2 - Au_1{}' u_2{}')$$

where m', $u_i{}'$ are the values of m and u_i which would have been obtained had the beam strength at that time been equal to I_H. However, from the above discussion and this definition we have

$$\text{(xvi)} \quad x'/I_H = x/I_c .$$

Also, since we take $u_i = a_i$, we have

$$\text{(xvii)} \quad u_i{}'/I_H = u_i/I_c .$$

Then from (xi)

$$\text{(xviii)} \quad m'/I_H = x'/I_H + 2\tau u_1{}' u_2{}'/I_H .$$

Substituting (xvi), (xvii) and (xiv) into (xviii) we get

$$\text{(xix)} \quad m'/I_H = m/I_c + (I_c - I_H)\, 2\tau u_1 u_2/I_c{}^2$$

To get y/I_H entirely in terms of data we substitute (xix) and (xvii) into (xv). The result is

$$\text{(xx)} \quad y/I_H = n/I_H - (1/I_c)\left[Am + 2\tau(v_1 v_2/R - Au_1 u_2)\right] .$$

We want the effect y/I_H in the form

$$\text{(xxi)} \quad y/I_H = n/I_H - zm/I_c .$$

By this definition and (xx) we have

$$z = A + (2\tau/m)(v_1 v_2/R - Au_1 u_2) . \qquad (4)$$

FIGURE CAPTIONS

Fig. 1. The geometry of the p-p type scattering experiments, showing the angles Φ and Θ relative to the beam and the contours of equal coincidence counting rate.

Fig. 2. Block diagram of the electronic apparatus.

Fig. 3. Fast pulse shaping circuit. Resistances are in ohms, 1/2 watt unless specified. Capacitances are in micromicrofarads, 400 w.v. Bypass and filter capacitors on the 150-volt line are not shown.

Fig. 4. Coincidence counts as a function of the voltage on one photomultiplier when the other photomultiplier was set at 750 volts. This photomultiplier was later operated at 800 volts.

Fig. 5 Coincidence counts as a function of the height of the scattering apparatus. The height units are approximately 10 to the inch. The apparatus was later set at height 35.5 .

Fig. 6 Hydrogen effect as a function of the angle between counters. The large peak is from elastic scattering; the smaller one from p-p type scattering. The angle subtended horizontally by each crystal was approximately 4 degrees.

Fig. 7 Coincidence rate due to inelastic scattering as a function of the angle between crystals. $\Phi = 45^{\circ}$. The angle subtended horizontally by the Θ crystal is approximately 10°.

Fig. 8 Resolving time of scalers for cyclotron beam pulses.

Fig. 9 Coincidences as a function of beam intensity. The dashed line gives $\tau = 1.0 \times 10^{-5}$ with an uncertainty of about 0.1×10^{-5} .

Fig. 10 Hydrogen effect as a function of the height of Θ crystal. $\Phi = 45^\circ$. h_o = 4.4 cm, 50 cm from target. $\Theta + \Phi = 86^\circ$.

Fig. 11 Summary of inelastic scattering results.

Fig. 12 Differential cross section for scattering of charged particles and curve used in obtaining the total cross section.

Fig. 13 Diagram illustrating the simplified kinematics for p-p type scattering. The ratio p/p' has been exaggerated for the sake of clarity.

Fig. 14 Geometry for scattering out of the plane of the scattering apparatus.

Fig. 15 Explanation in text (page 31).

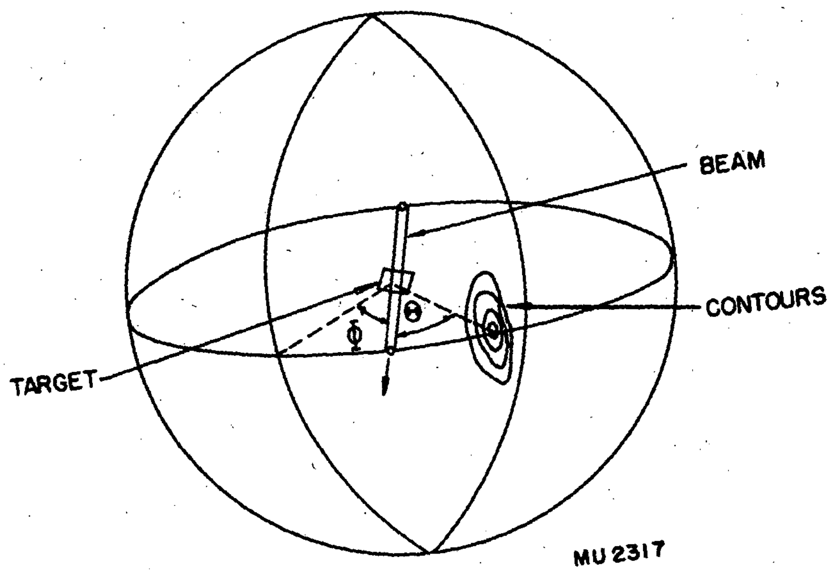

Fig. 1

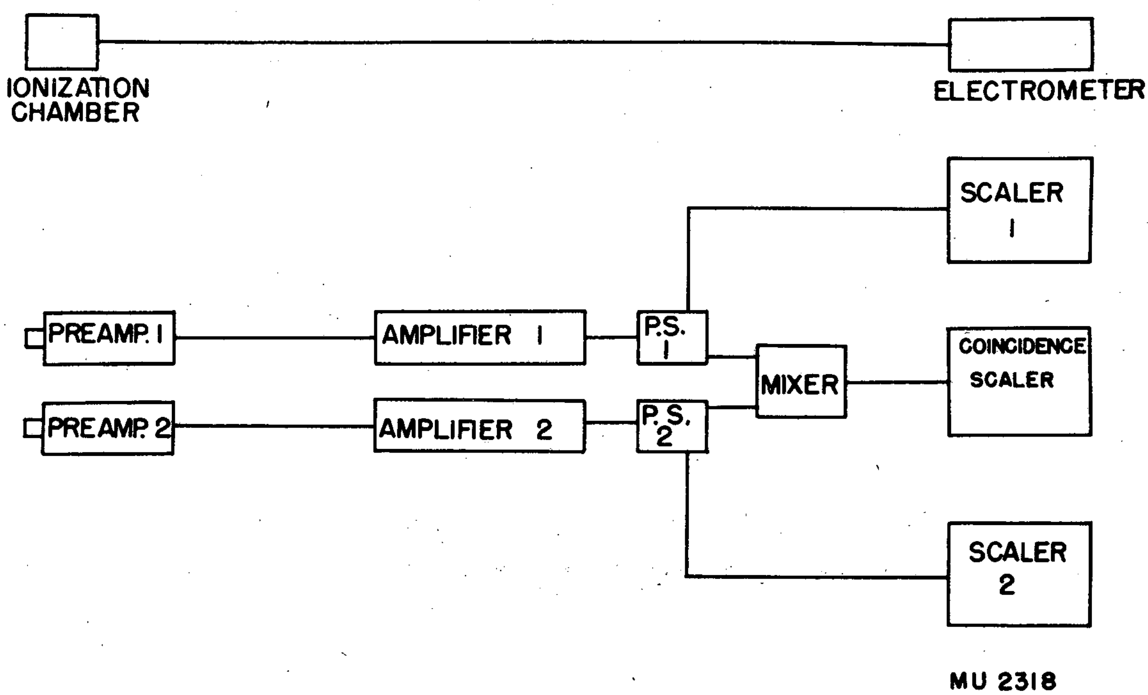
IONIZATION CHAMBER
ELECTROMETER
SCALER 1
PREAMP. 1
AMPLIFIER 1
P.S. 1
MIXER
COINCIDENCE SCALER
PREAMP. 2
AMPLIFIER 2
P.S. 2
SCALER 2
MU 2318

Fig. 2

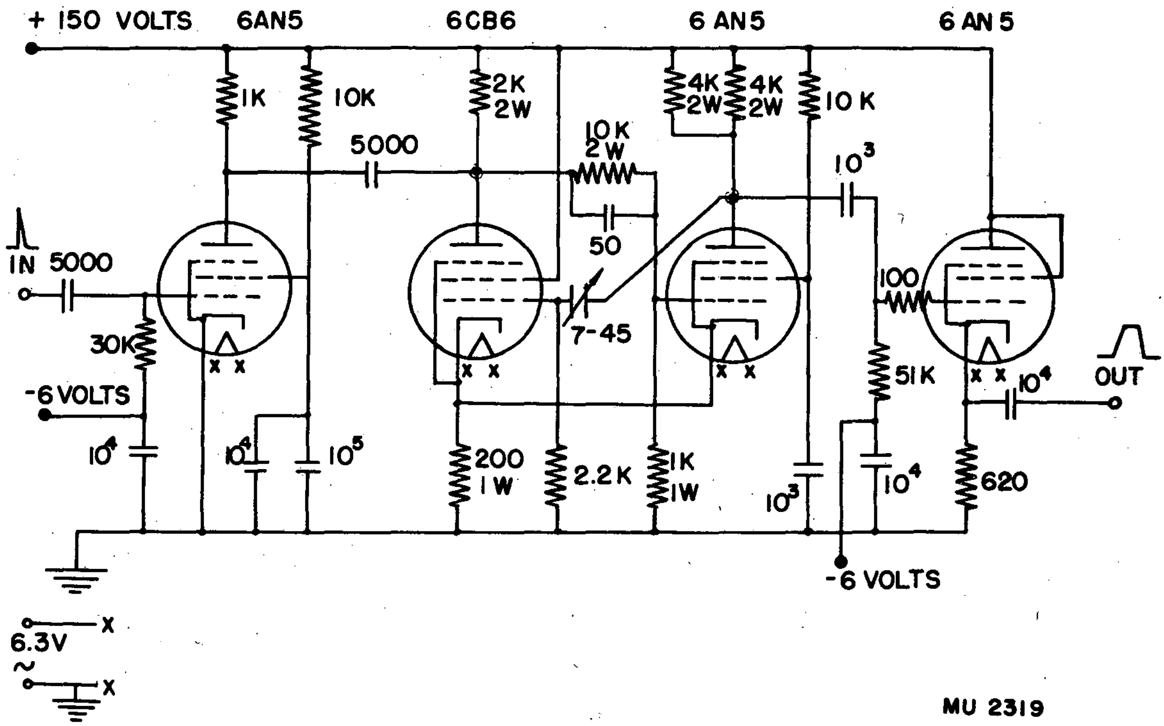
+ 150 VOLTS
6AN5
6CB6
6 AN5
6 AN 5
1K
10K
5000
2K
2W
10 K
2W
50
4K
2W
4K
2W
10 K
10^3
IN
5000
30K
-6 VOLTS
10^4
10^4
10^5
7-45
100
51 K
10^4
OUT
200
1W
2.2 K
1K
1W
10^3
10^4
620
-6 VOLTS
6.3V
~
MU 2319

Fig. 3

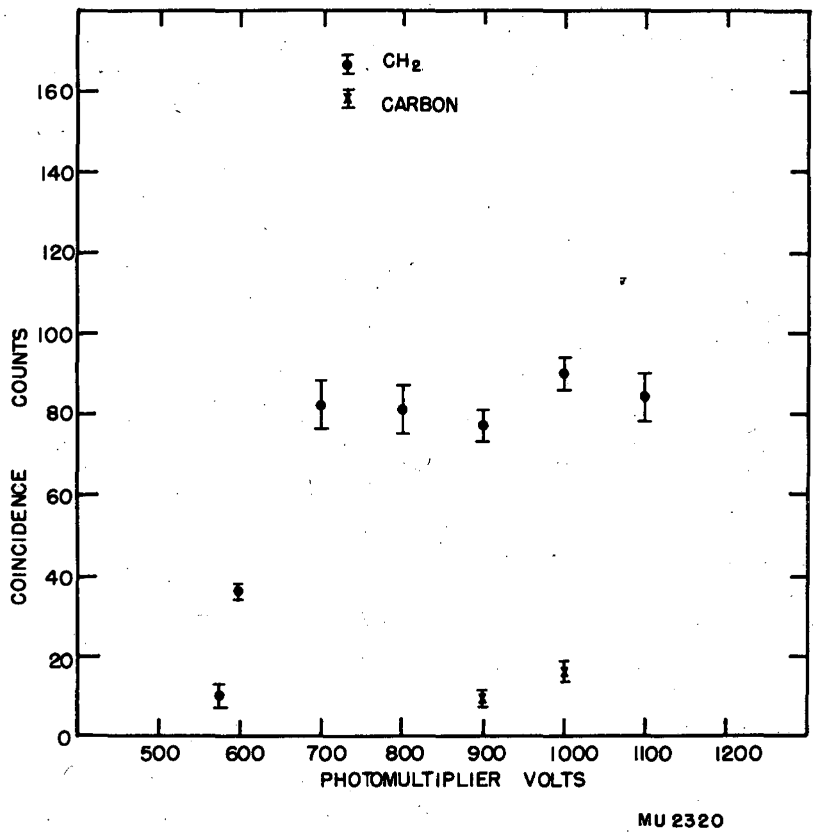
CH2
CARBON
COINCIDENCE COUNTS
0
20
40
60
80
100
120
140
160
500
600
700
800
900
1000
1100
1200
PHOTOMULTIPLIER VOLTS
MU 2320

Fig. 4

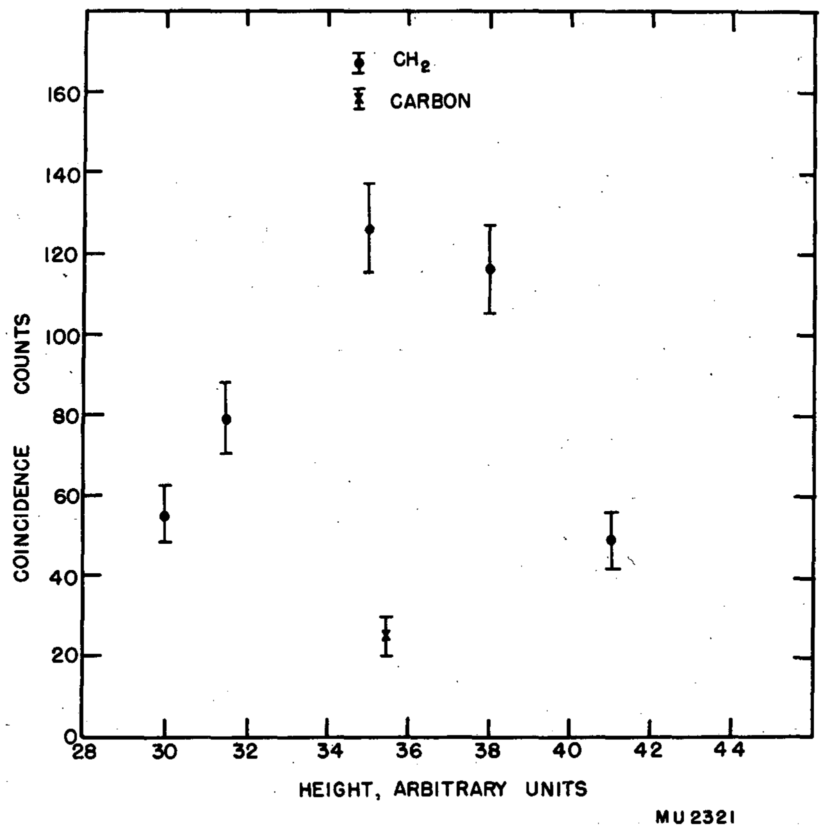

CH2
CARBON
160
140
120
100
80
60
40
20
0
COINCIDENCE COUNTS
28
30
32
34
36
38
40
42
44
HEIGHT, ARBITRARY UNITS
MU 2321

Fig. 5

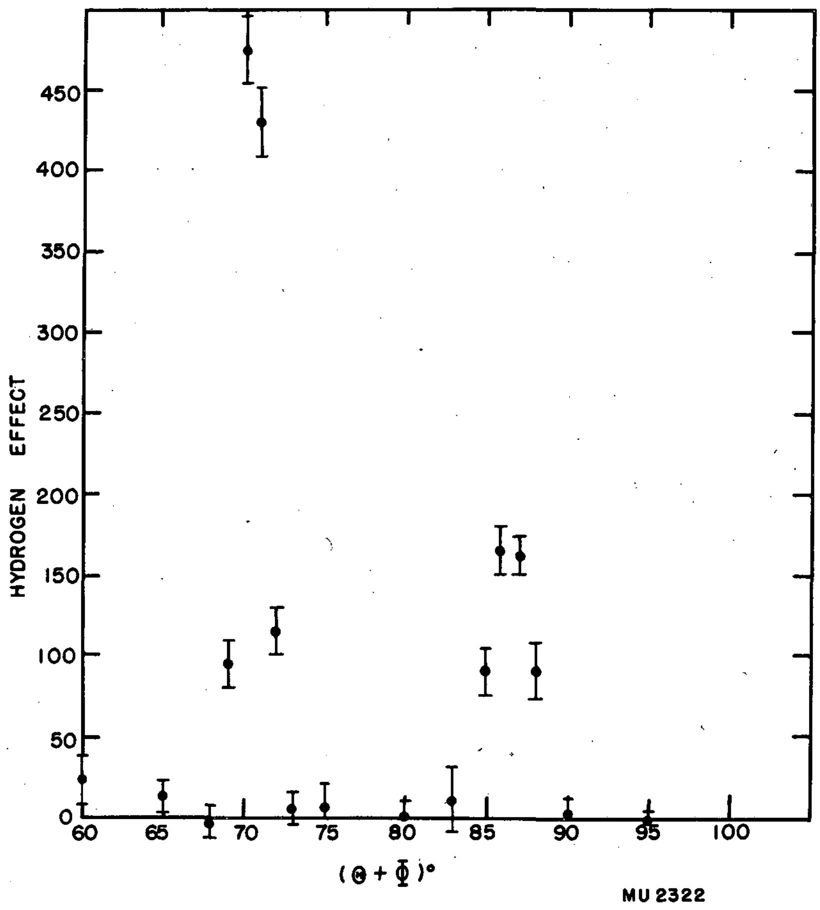

HYDROGEN EFFECT
0
50
100
150
200
250
300
350
400
450
60
65
70
75
80
85
90
95
100
(Θ + Φ)°
MU 2322

Fig. 6

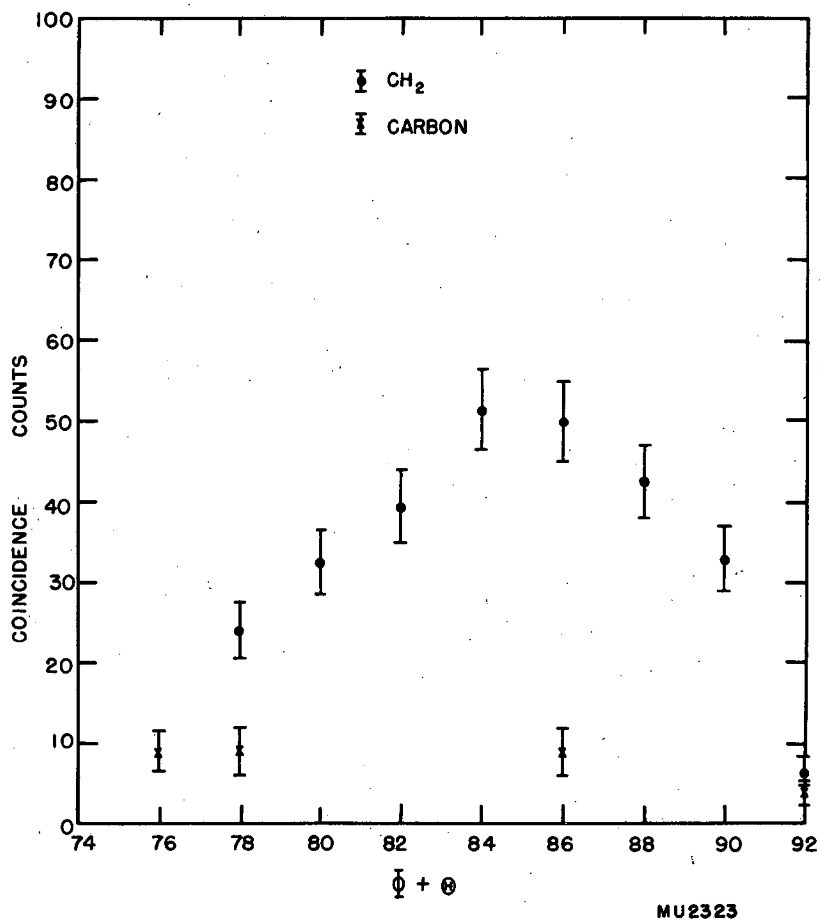

100
90
80
70
60
50
40
30
20
10
0
COINCIDENCE COUNTS
CH_2
CARBON
74
76
78
80
82
84
86
88
90
92
$\Phi + \Theta$
MU2323

Fig. 7

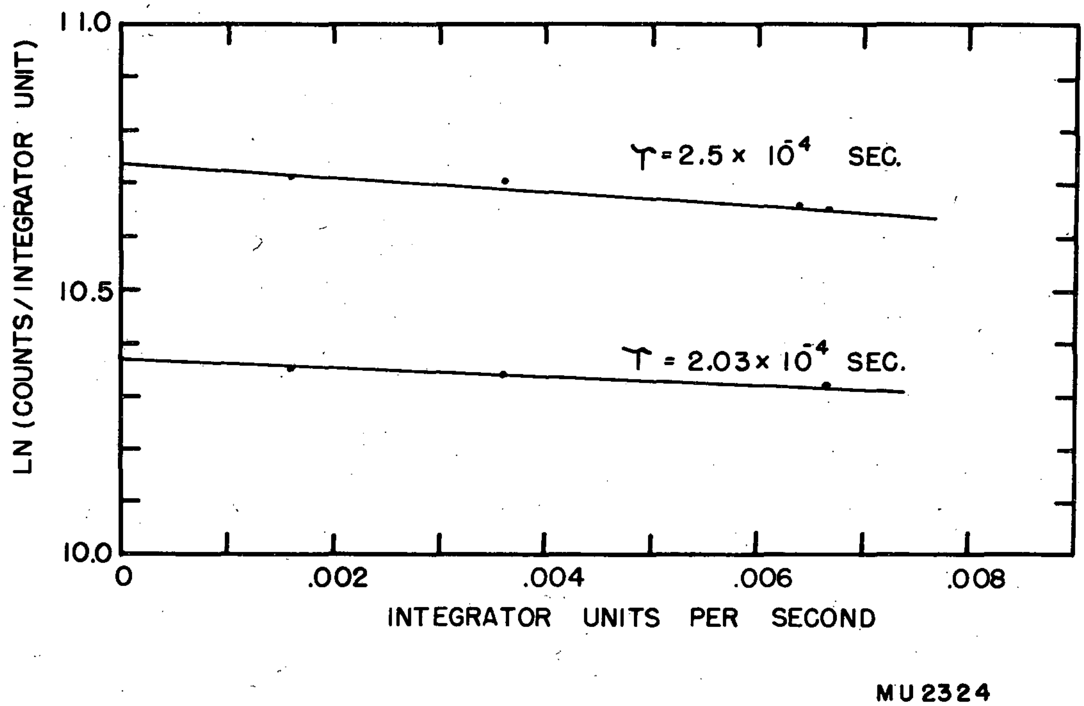

11.0
10.5
10.0
LN (COUNTS/INTEGRATOR UNIT)
τ = 2.5 × 10⁻⁴ SEC.
τ = 2.03 × 10⁻⁴ SEC.
0
.002
.004
.006
.008
INTEGRATOR UNITS PER SECOND
MU 2324

Fig. 8

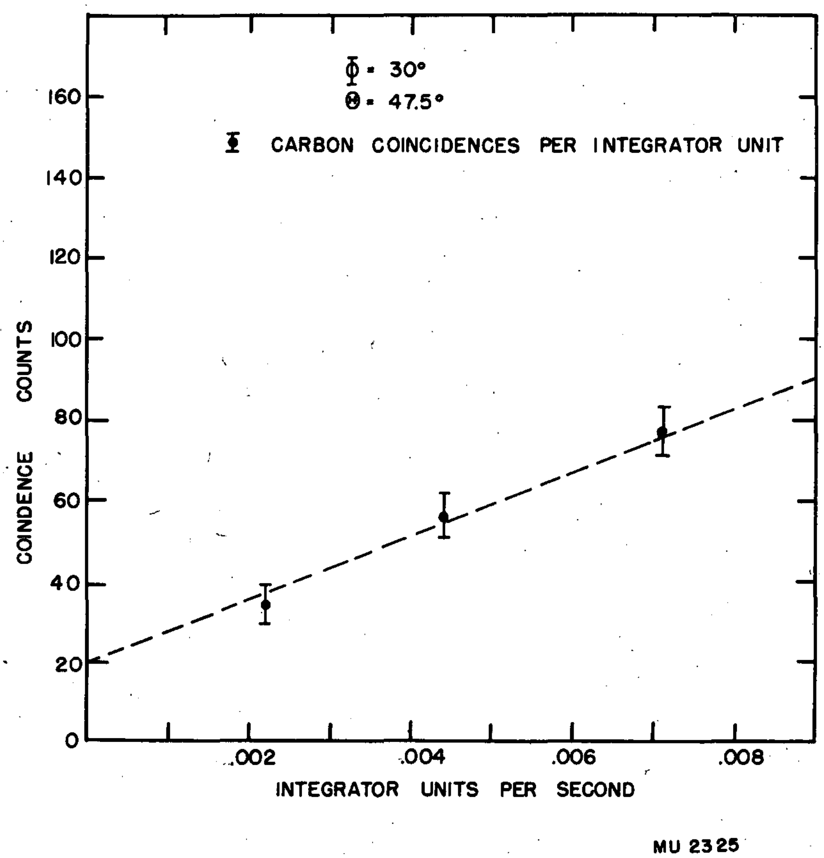

Φ = 30°
Θ = 47.5°
CARBON COINCIDENCES PER INTEGRATOR UNIT
CONIDENCE COUNTS
INTEGRATOR UNITS PER SECOND
0
20
40
60
80
100
120
140
160
.002
.004
.006
.008
MU 2325

Fig. 9

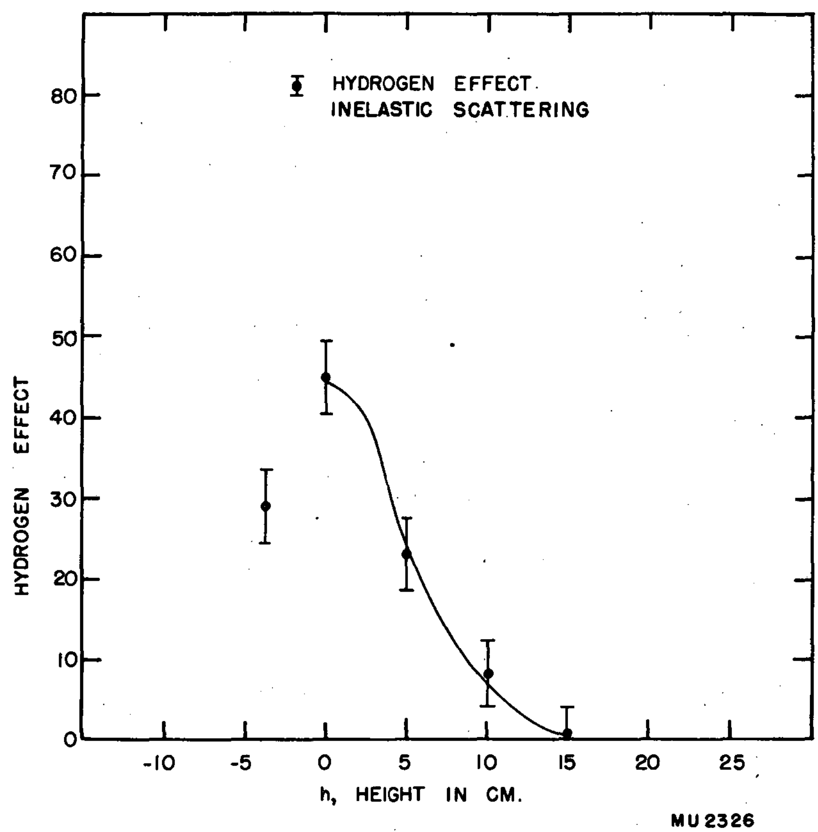
HYDROGEN EFFECT
INELASTIC SCATTERING
80
70
60
50
40
30
20
10
0
HYDROGEN EFFECT
-10
-5
0
5
10
15
20
25
h, HEIGHT IN CM.
MU 2326

Fig. 10

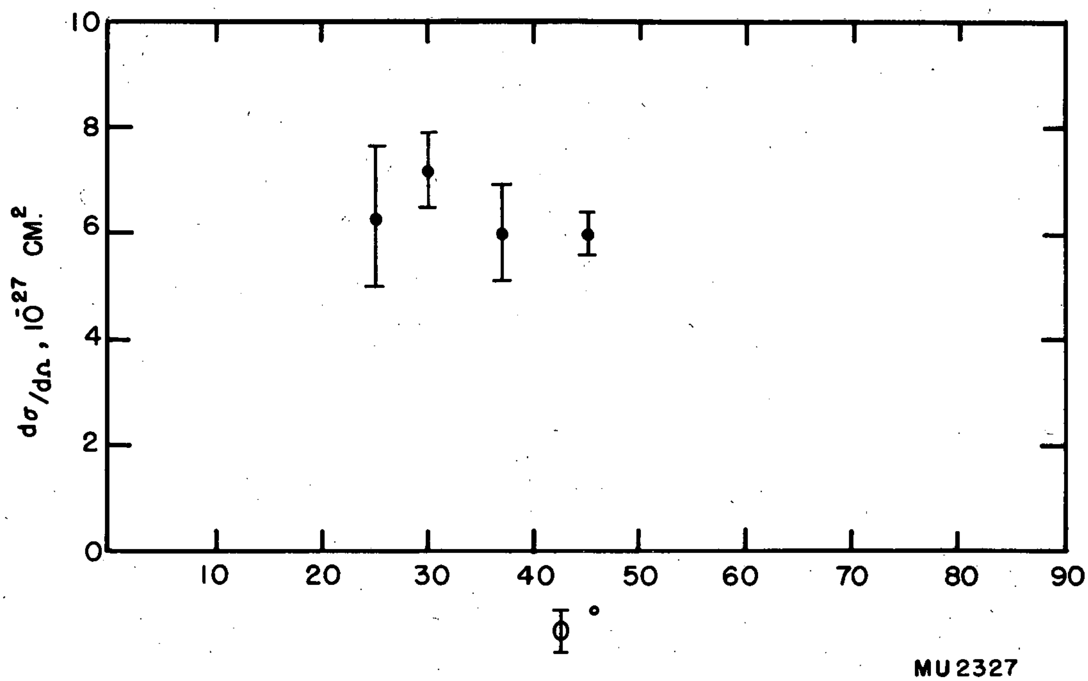

Fig. 11

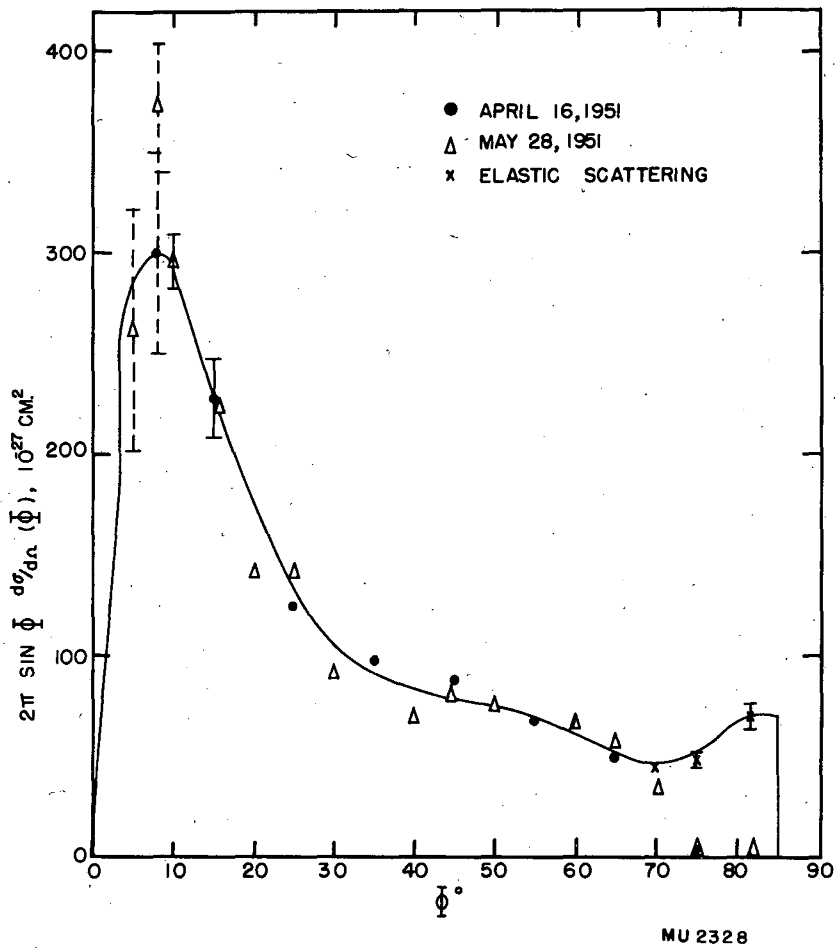

400
300
200
100
0
2π SIN Φ dσ/dΩ (Φ), 10^{27} CM.²
APRIL 16, 1951
MAY 28, 1951
ELASTIC SCATTERING
0
10
20
30
40
50
60
70
80
90
Φ°
MU 2328

Fig. 12

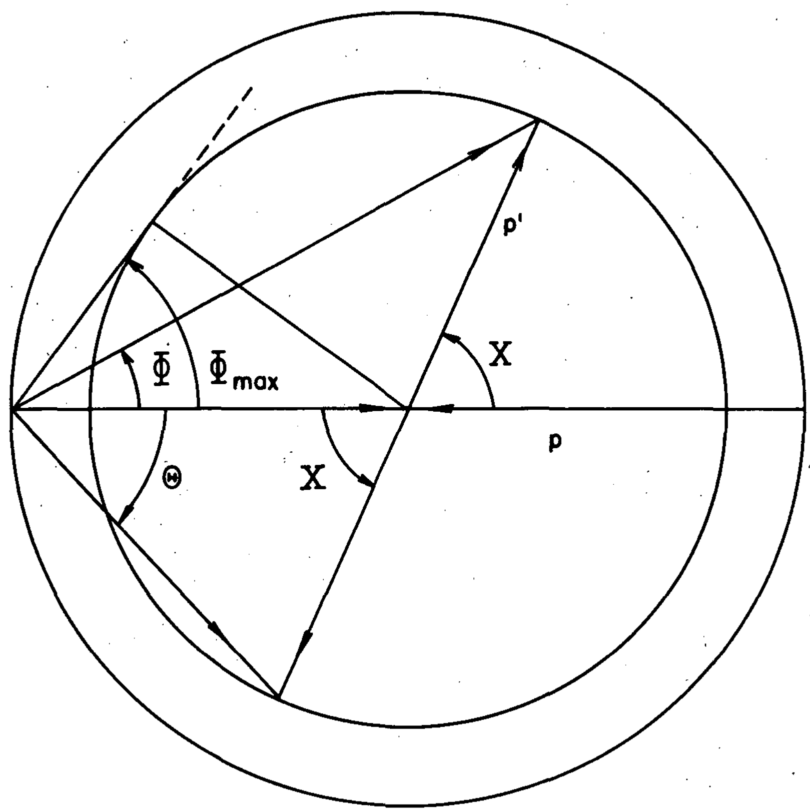

Fig. 13

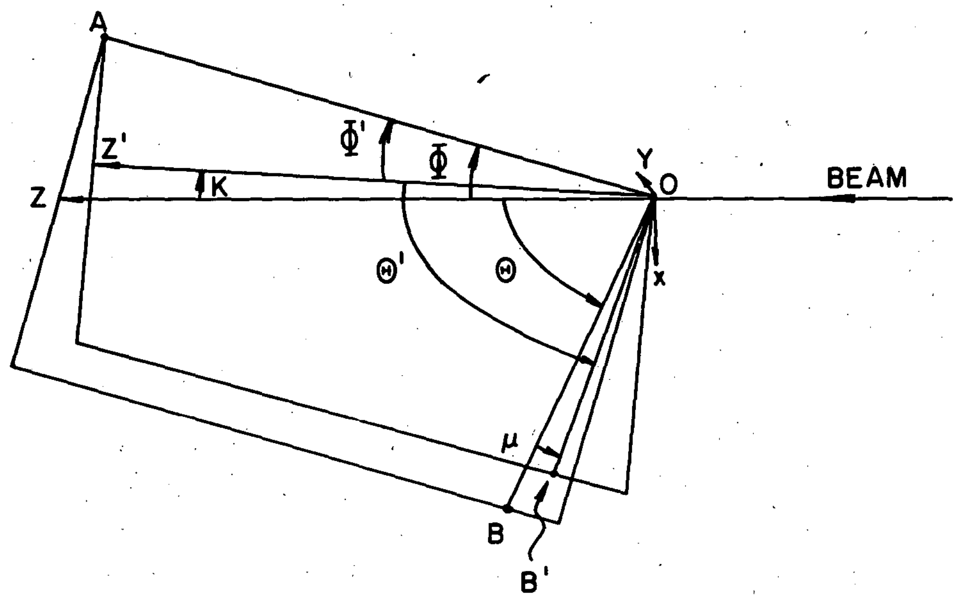

MU 2330

Fig. 14

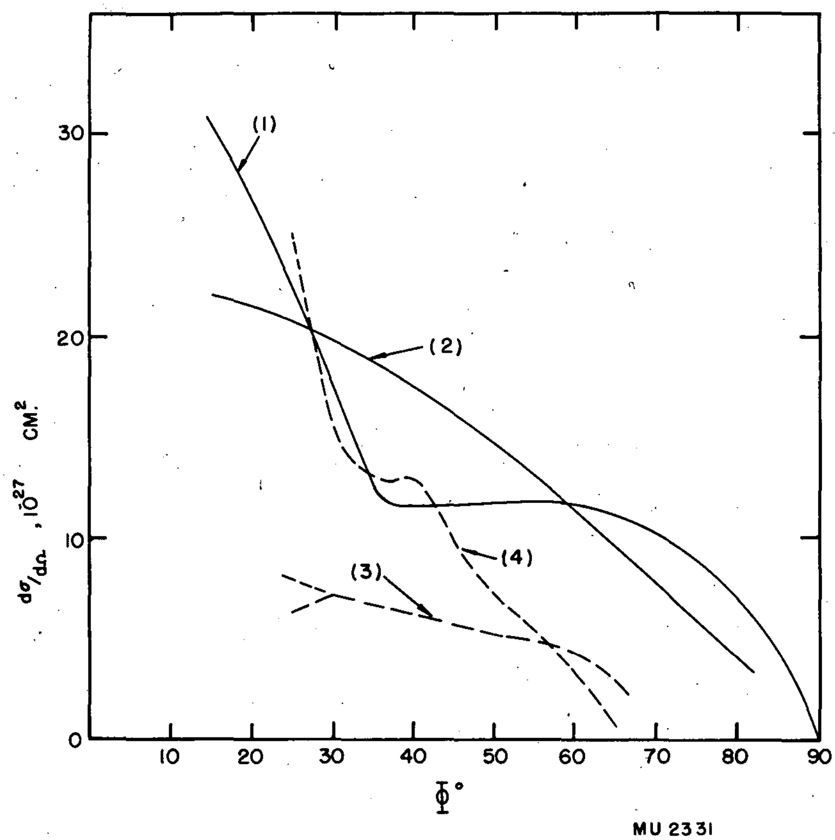

(1)
(2)
(3)
(4)
30
20
10
0
$d\sigma/d\Omega$, 10^{-27} CM.^{2}
10
20
30
40
50
60
70
80
90
$\Phi°$
MU 2331

Fig. 15